ISSN 0016-8521, Geotectonics, 2016, Vol. 50, No. 5, pp. 522–533. © Pleiades Publishing, Inc., 2016.
Original Russian Text © E.A. Rogozhin, A.I. Lutikov, Tuo Shen, 2016, published in Geotektonika, 2016, No. 5, pp. 82–94.

Tectonic Position and Geological and Seismic Manifestations of the Gorkha Earthquake of April 25, 2015, in Nepal

E. A. Rogozhin*, A. I. Lutikov, and Tuo Shen

Schmidt Institute of Physics of the Earth, Russian Academy of Sciences, ul. Bol'shaya Gruzinskaya 10, Moscow, 123242 Russia

**e-mail: eurog@ifz.ru*

Received January 14, 2016

Abstract—The characteristics of sources of the Gorkha earthquake's mainshock (April 25, 2015, Nepal) and strongest aftershock are given. Macroseismic data and examples of seismic dislocations are provided. The course of seismic energy release during the aftershock process is analyzed. The data on seismological precursors of the mainshock and the strongest aftershock of May 12, 2015, are presented, which allowed the aftershock to be predicted in a short-term interval.

Keywords: source, seismicity, Earth's crust, faults, earthquake, thrust, mainshock, aftershock, paleoseismogeology, seismic dislocations

DOI: 10.1134/S0016852116050046

INTRODUCTION

On April 25, 2015, at 06:11 GMT, a catastrophic earthquake occurred in Nepal; this event was called Gorkha. The moment magnitude of this earthquake was $M_W = 7.9$. Based on the data of the Service for Emergency Messages, Geophysical Survey of the Russian Academy of Sciences (SEM GS RAS), the epicenter of the mainshock was located at 28.18° N, 84.78° E. The depth of the hypocenter was 15 km.

The earthquake killed 9000 people and injured 14500; many buildings were destroyed in Kathmandu, the capital of Nepal. Considerable damage was done to the historical center of Kathmandu. Eighty climbers were killed on Mt. Everest from avalanches triggered by the earthquake. Tremors were felt in the neighboring countries of China, India, Pakistan, and Bangladesh, where there were more than 100 casualties.

The instrumentally determined epicenter was located in Nepal (Fig. 1), 75 km northwest of Kathmandu.

Figure 1 shows a map of the epicenters of strong earthquakes ($M_W \geq 5.8$) in the central and eastern Himalayas that occurred in the period of 1911–2015 (111 seismic events in total). To compile this map, the USGS catalog (USGS, NEIC) was used. The strongest earthquake in the region was the M_W 8.4 Bikhar–Nepal earthquake of January 15, 1934, with the epicenter located in India, in the southern part of the considered Himalayan region.

The 1988 earthquake had a magnitude of $Ms = 6.6$, and its epicenter was located south of the abovementioned 1934 event (see Fig. 1).

The epicenter of the Gorkha earthquake that occurred on April 25, 2015, was located west of the sources of these two strong seismic events, closer to the central part of the Himalayan mobile system.

There are a number of non-Russian scientific publications about different manifestations of this seismic event [6–9, 11, 14, 17, 19]. In Russia, there are only a few scientific works describing the results of seismological studies of the catastrophic event in Nepal [3]. We have collected and analyzed the literature and instrumental data on surface manifestations of the earthquake proper and its precursors, on the structure and slip type, and the course of the aftershock process.

MAINSHOCK PRECURSORS

During seismological observations of the current seismicity, the source zone of the Gorkha earthquake was characterized by lower seismic activity for all recent years: a quiescent zone at about 28° N between 84.5° and 86.5° E. Its approximate size is 250 × 70 km^2 [18] (Fig. 2). Analysis of the distribution of weak and moderate earthquakes in this part of the Himalayan region in 1982–1985 [5] and 1994–1998 [22] has shown the presence of a seismic gap in northeast Nepal. In these periods, local seismic networks (5 stations for the former period and 17 stations for the latter) recorded more than 10000 earthquakes, whose epicenters demonstrated more or less similar distributions of active zones. Seismicity is clustered in the frontal ridges of the High Himalayas in the depth range of 10–20 km. The most abundant manifestations of seismicity were reported in western (west of

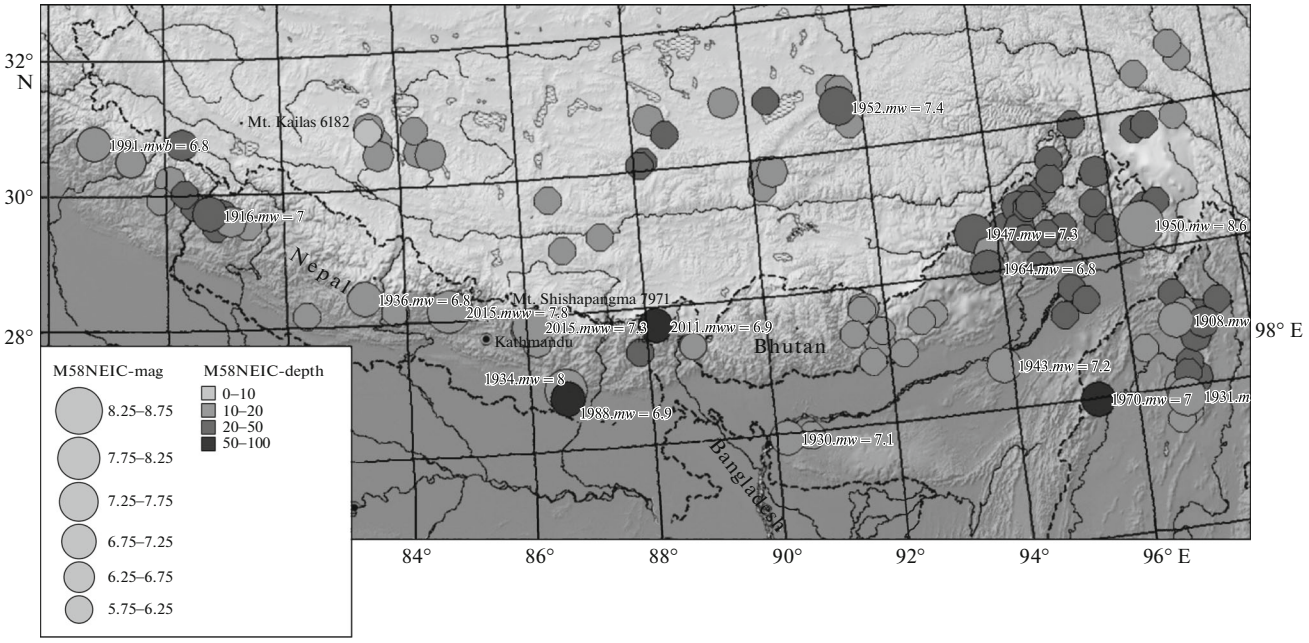

Fig. 1. Map showing epicenters of strong ($M_W \geq 5.8$) earthquakes in Himalayan region (1911–2015) in region of $25.5° \leq \varphi \leq 31.0°$ N, $75.0° \leq \lambda \leq 98.0°$ E. Hypocentral depths of earthquakes are also indicated.

82° E) and eastern Nepal (between 86° and 88° E) [22]. There were almost no epicenters in the source zone of the 2015 Gorkha earthquake, whereas the instrument-determined epicenter of this earthquake was located near the northwestern boundary of the seismic quiescence zone (see Fig. 2).

These seismic gaps also exist in other segments of this mountain-folded system. For example, the contemporary seismic quiescence zone has been reported in the western and central Himalayas: according to paleoseismogeological data, strong earthquakes occur there with an average recurrence interval of 700–800 years [4, 15, 23].

Thus, the strong earthquake in Nepal had long-term seismological precursors.

MACROSEISMIC MANIFESTATIONS

According to the USGS data, the highest macroseismic effect was VIII on the modified Mercalli scale (Fig. 3). Within the zone of I = VIII, particular settlements with I = IX were reported, but the isoseismal of I = IX could not be mapped. The zone with I = VIII covered the foothills and southern slope of the High Himalayas and had an irregular oval shape; the major axis of this oval was WNW-oriented, in parallel to the trend of mountain ranges. The length of this zone was about 150 km, and the width was 60–70 km. The zone of maximum shaking included Kathmandu and such big cities as Panaoti (population is 28000), Bharatpur (107000), and Banepa (17000).

The zone with I = VII was almost isometric and irregular in shape, slightly WNW-elongated and occupying almost all of central Nepal from its boundary with China in the north-northeast to that with India in the south-southwest. Its length and width were about 200 and 180 km, respectively. This zone partly covered boundary regions of India.

Beyond the central part of Nepal, shaking with I = VI was reported in vast areas of India (at the boundary with Nepal) and in southern areas of southwest Tibet. The isoseismal of I = VI was curved in a very complex way and framed an area approximately 400 × 400 km^2 in size.

SURFACE DEFORMATIONS

Such primary seismic dislocations as seismic ruptures, which appear during the mainshock, have not been found on the surface. This means that the source did not reac the surface and was "blind," like many other earthquake sources in the Himalayas. In contrast, multiple secondary deformations manifested themselves. The earthquake triggered many rock falls and landslides on steep slopes, vibration cracks in road pavement (Figs. 4 and 5), and snow avalanches in the High Himalayans (Fig. 6). These seismic dislocations were observed on all slopes prone to these phenomena within the isoseismal of I = VIII [7, 14].

Operational investigation of the epicentral zone by American researchers has revealed 4312 coseismic and postseismic landslides, as well as several dam lakes formed after large rock falls [14]. The distribution den-

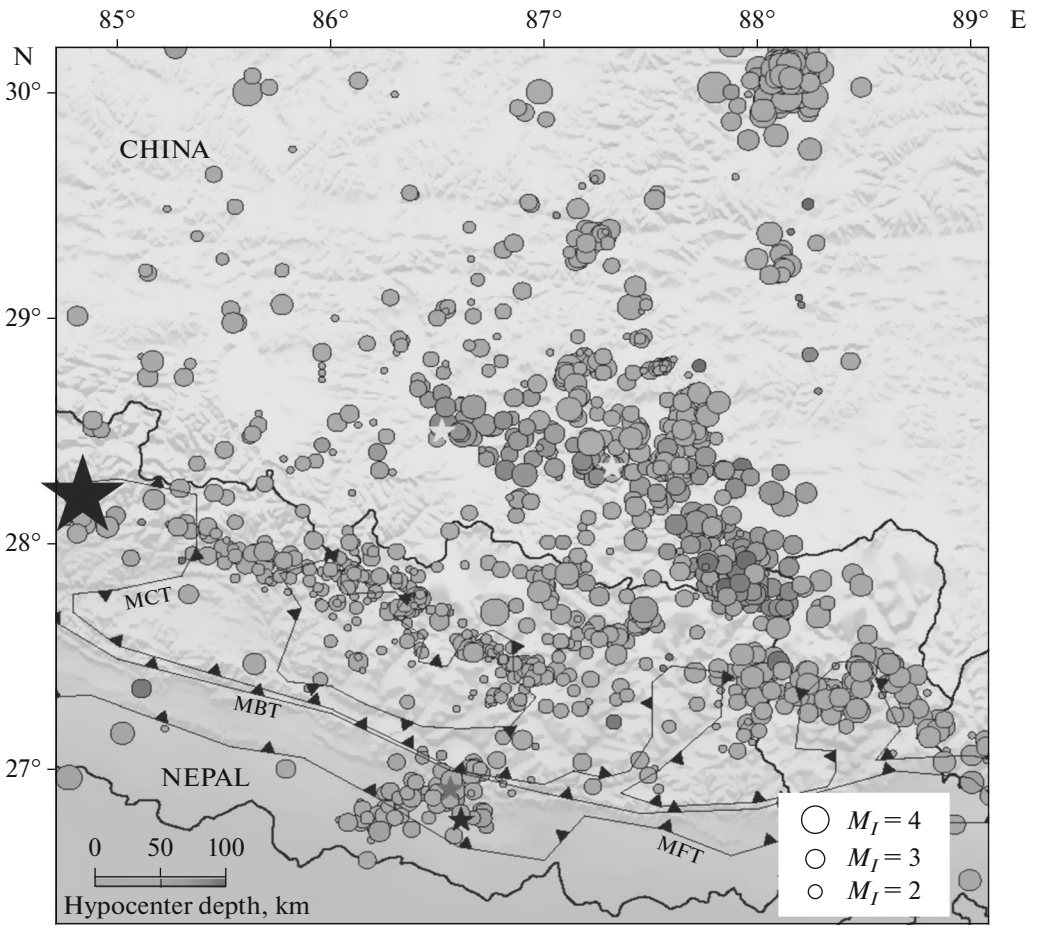

Fig. 2. Map showing epicenters of weak and moderate (M_I = 2–4) earthquakes in Himalayas within boundaries of Nepal and intermountain trough, based on data from digital telemetric seismic network [18] with modifications. Small black and gray stars denote epicenters of strongest 1934 and 1988 earthquakes, respectively; light gray asterisks, epicenters of noticeable earthquakes in southern Tibet. Large asterisk marks epicenter of mainshock of 2015 Gorkha earthquake. Abbreviations denote main regional faults: MBT, Main Boundary Thrust; MFT, Main Frontal Thrust; MCT, Main Central Thrust.

sity of landslides over the surface correlates with the steepness of slopes, sites of peak ground acceleration, subsiding areas of the Earth's surface, outcrops of metamorphic rocks pertaining to specific types, and large outcropping intrusions. In general, the majority of catastrophic slope phenomena was observed in the shaking zone of I = VIII.

In the Kathmandu valley, a few cases of soil liquefaction were also revealed.

SIZE OF MAINSHOCK SOURCE, SEISMOTECTONIC POSITION OF THE SOURCE ZONE, AND CHARACTER OF SEISMOGENIC SLIP

The size of a source is determined from the distribution of aftershocks that occurred in the first months after the mainshock (Fig. 7). According to these data, the projection of the source on the surface is oval in shape, with a length of about 160–170 km and width of about 70–80 km. The majority of aftershock hypocenters were located within the range of 0–15 km. The type of slip can be dtermined from an analysis of the mainshock's focal mechanism (Fig. 8a). For this, we used the calculation results from database [27]. The pressure axis was oriented SSW–NNE across the trend of the Nepal segment of the Himalayan mobile system and dipped to the NNE at an angle of 30°. The tension axis had nearly the same direction and dipping angle (SSW-oriented, dipping at about 60°). One of the alternative planes dipped gently (at 10°–20°) to the NNE, whereas another dipped steeply (at about 70°) to the SSW. Small hypocentral depths of the mainshock and the majority of aftershocks make it possible to select the gentle plane, which dips beneath the Himalayan mobile system, as the active one. In such a case, the type of slip was thrusting of the High Himalayas onto the Low Himalayas and foothills, with an insignificant right-lateral strike-slip component.

The validity of such a choice is indicated by the results of works carried out with an interferometric synthetic aperture radar (InSAR) [17]. According to

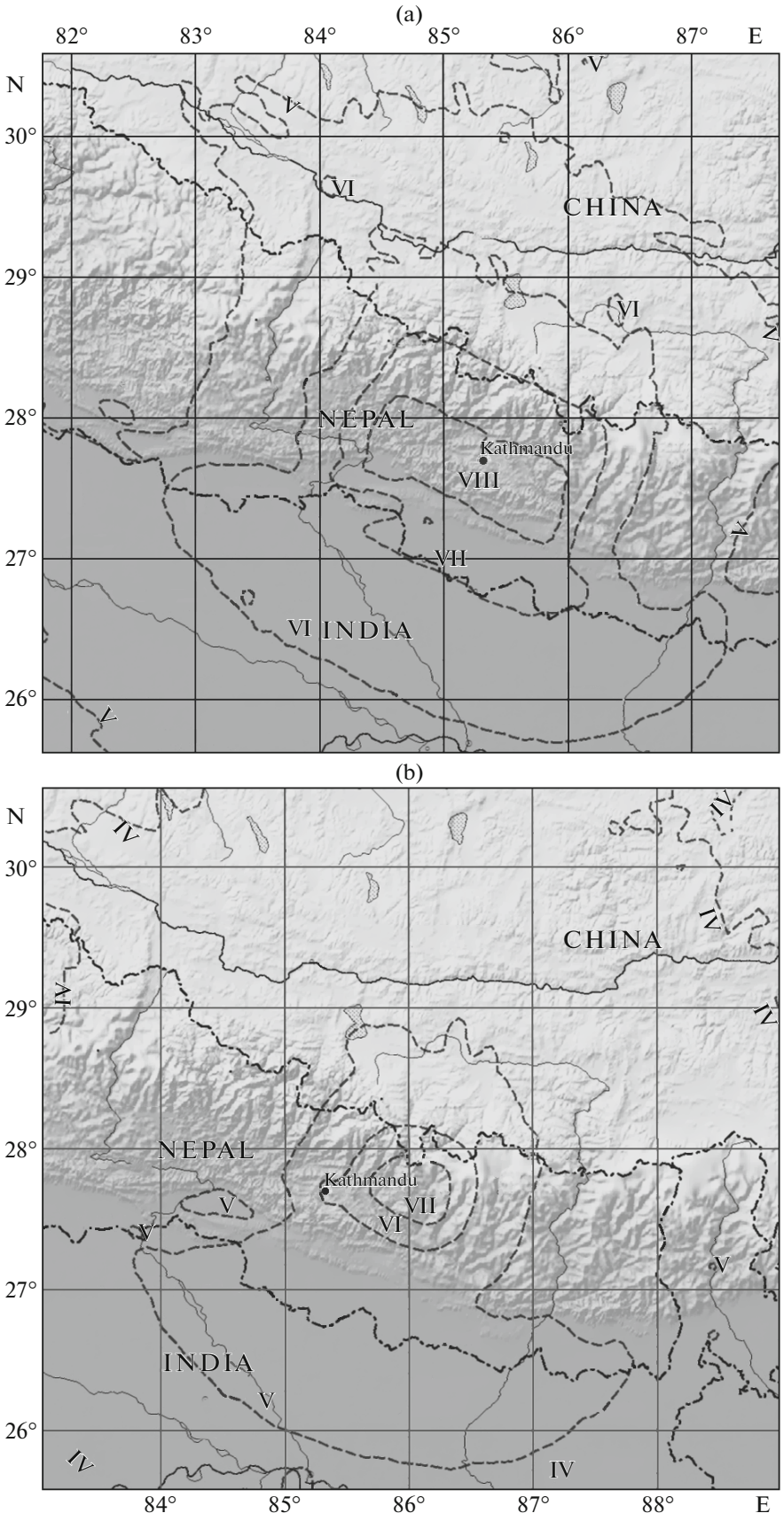

Fig. 3. Isoseismal map for highest shaking of mainshock (a) and strongest aftershock of May 12, 2015 (b) based on USGS data [30].

Fig. 4. Crown cracks on gully slopes.

Fig. 5. Vibration cracks on road in High Himalayas.

Fig. 6. Avalanche in High Himalayas.

these data, the earthquake caused the zone of High Himalayas to uplift by approximately 0.7–1.0 m, whereas the depression dividing the High and Low Himalayas also subsided by approximately 0.5–1.0 m. The low Himalayas and southern foothills did not suffer any significant vertical motions (Fig. 9) [6, 9]. These data agree with the results of gravity anomaly analysis [8]. Reconstruction of horizontal thrusting motions in the source yielded values from 1.5 to 3.5 m in different parts of the active plane [28].

The active plane in the source spatially fits the zone of the Main Boundary Thrust of the Himalayas (MBT) that gently dips northward [5, 10, 20–22, 25, 26]. This thrust divides the tectonic zones of the High Himalayas in the north and the Low Himalayas in the south from the foothill zone. With depth, the thrust gains a listric (overthrust) structure and gently dips beneath the Himalayan mobile system. It is this gently dipping part of the fault zone that played the role of the seismogenic structure.

The MBT has repeatedly generated the strongest earthquakes in the Himalayan region in the past. Paleoseismological studies in western Nepal and in the zones of the MBT and the adjacent Main Frontal Thrust (MFT) have revealed primary seismic ruptures produced by the strongest seismic events of the last 5000 years. Quakes with magnitudes about 8 occurred seven times in this period. Their recurrence interval was 870 ± 350 to 750 ± 140 years [4, 16].

Some researchers attribute the source of the Gorkha earthquake as hosted on the Main Central Thrust (MCT) located further north. Due to the small dipping angle, the outline of this fault within the mountainous area is highly curved in plan view (see Fig. 9). However, the mainshock's epicenter appears to be south of the area where this thrust reaches the surface, so there is no reason to think the Gorkha earthquake hypocenter was located on this fault.

There is a common idea that strong earthquakes in the Himalayas, if their active planes gently dip toward Tibet, cause underthrusting of the Indian Plate beneath the mobile mountain system, instead of overthrusting of the Himalayas above India [12, 20]. Such an interpretation is supported by the geological and geomorphological data on the activation of a number of recent submeridional grabens in the southern fore-Himalayan zone of Tibet [24].

OPERATIONAL ANALYSIS OF THE AFTERSHOCK PROCESS

Operational analysis of the aftershock process has been carried out since April 25, 2015, in a nearly online regime based on data from the catalog by SEM GS RAS [29] and the Quick CMT catalog [30]. During the first three days after the mainshock, two strong aftershocks with M_W = 6.7 and 6.8 were recorded. On the whole, on April 25–27, GS RAS recorded 37 aftershocks with $mb \geq 4.3$. Figures 10 and 11 show the maps of the aftershock distribution for the earthquake of April 25, based on SEM GS RAS data for the first hours and the first day after the mainshock.

According to Fig. 11 and judging by the aftershock cloud of the first day, the earthquake source extended WNW–ESE with a length and width of about 160–170

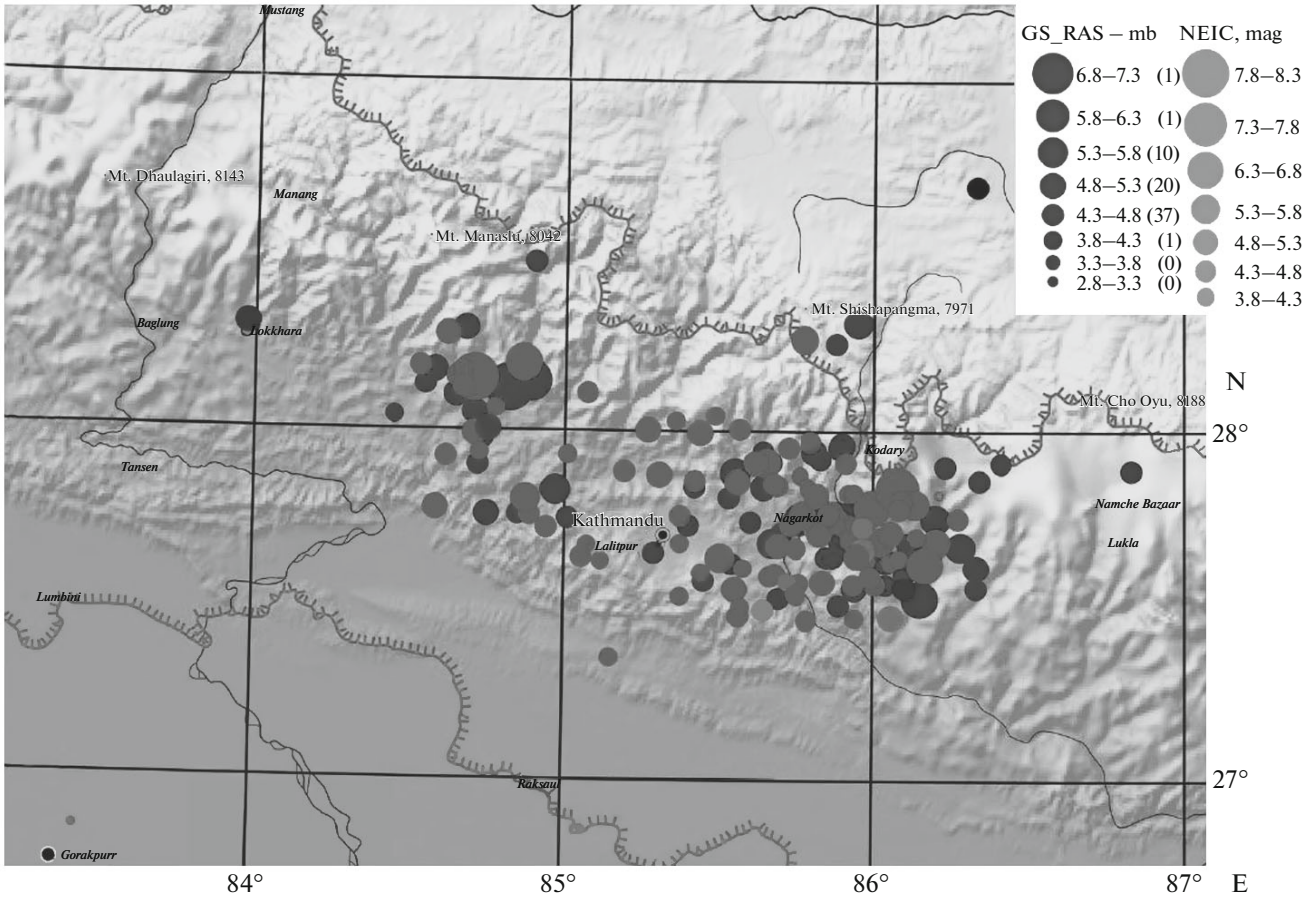

Fig. 7. Epicentral map for mainshock and aftershocks of Gorkha earthquake of April 25, 2015, as of September 29, 2015. Darker tone marks events recorded by GS RAS; lighter tone, events from USGS catalog. Circles with different diameters correspond to epicenters with different magnitudes.

and 50–60 km, respectively. Rupturing in the source began in its WNW part and propagated ENE. Thus, it was as though aftershocks were filling the above-mentioned seismic quiescence zone to the south and southeast from the instrument-determined position of the epicenter of the April 25 mainshock (see Fig. 2).

Figure 12 shows the release the cumulative scalar seismic moment ($M_{0\text{cum}}$) with the aftershocks, expressed in fractions of the scalar seismic moment of the mainshock (main event; $M_{0\text{me}}$) for the period of 66 h from the main event. It is seen that the seismicity is quite weak between the aftershocks, and on April 28 (until 18:00 GMT), there were no significant earthquakes with $mb \geq 4.3$. The absence of noticeable aftershocks for 18 h can be interpreted as a phase of seismic quiescence within the aftershock sequence before the new strong aftershock.

Note that virtually every strong earthquake ($M_W > 7.0$) is succeeded by a more or less long phase of quasistationary release of the scalar seismic moment with the aftershocks. A similar pattern was observed, for example, after the mainshocks of the Olyutora earthquake (April 20, 2006; $M_W = 7.6$) in Koryakiya [1], the Tohoku earthquake (March 11, 2011; $M_W = 9.1$) in Japan [2], and many other strong earthquakes. The duration of the quasistationary phase of M_0 release depends on the magnitude of the mainshock: the

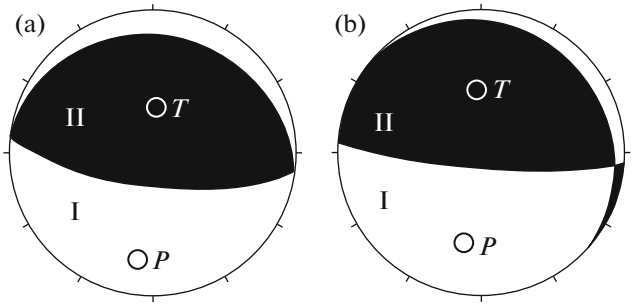

Fig. 8. Stereograms showing solutions of focal mechanisms [27] for mainshock (a) and strongest aftershock of May 12, 2015 (b). Projection to lower hemisphere. Black field denotes zone of pressure stress; white, tension stress. Black and white dots denote positions of tension and pressure stress axes, respectively.

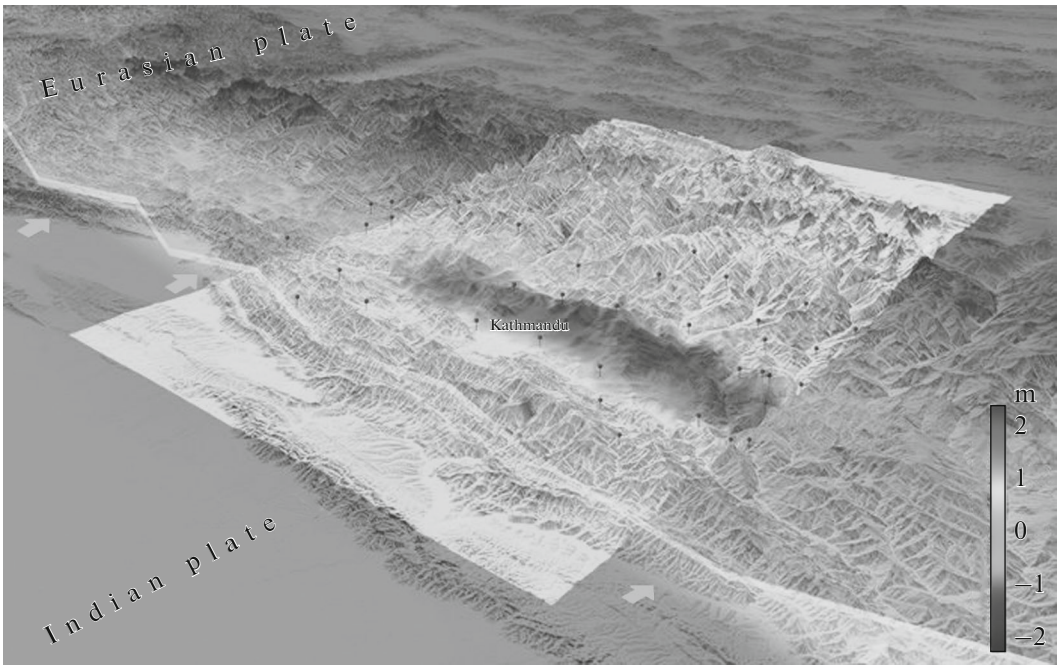

Fig. 9. Scheme of vertical displacements of surface by InSAR method [17], with Indian and Eurasian lithospheric plates indicated.

greater the magnitude, the longer the duration. For example, this phase lasted 32 days for the $M_W = 7.6$ Olyutora earthquake, whereas for the Tohoku megaearthquake with $M_W = 9.1$, the quasistationary phase of the aftershock process was observed for more than seven months. The duration of the quasistationary phase of seismic moment (M_0) release likely does not exceed 10–15% of the total duration of the aftershock sequence. We should also note that the presence and duration of the quasistationary phase of M_0 release

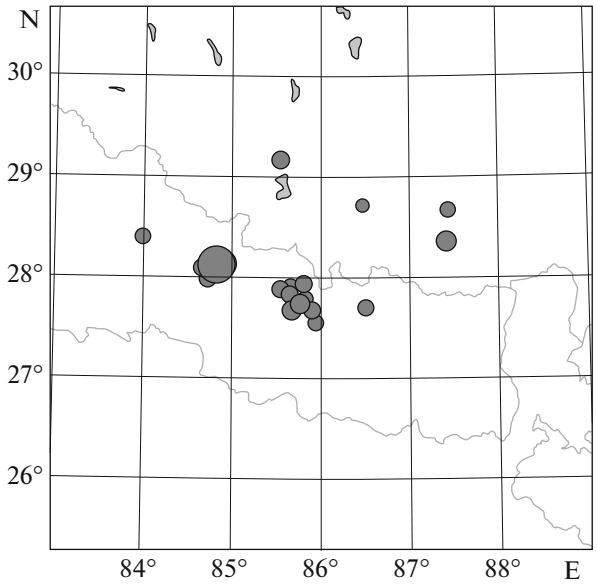

Fig. 10. Map showing locations of epicenters for aftershocks that occurred in first few hours after April 25 mainshock, according to SEM GS RAS. Mainshock epicenter (06:11:23 GMT) is marked with largest circle in eastern part of epicentral field. Smaller circle that almost matched position of mainshock denotes epicenter of strongest aftershock ($M = 6.8$, April 25, 2015; 06:45:19 GMT).

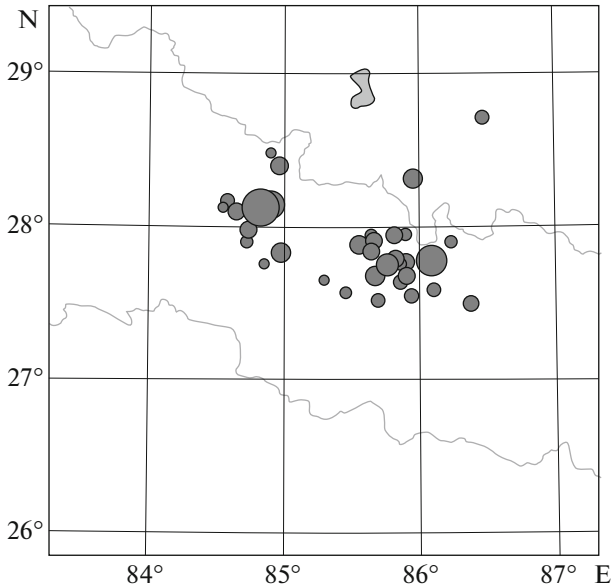

Fig. 11. Map showing locations of epicenters for aftershocks that occurred on first day after April 25 mainshock, according to SEM GS RAS. The mainshock's epicenter is marked with the largest circle. Smaller circle in eastern part of epicentral field denotes location of strong aftershock of April 26 (07:09:06 GMT).

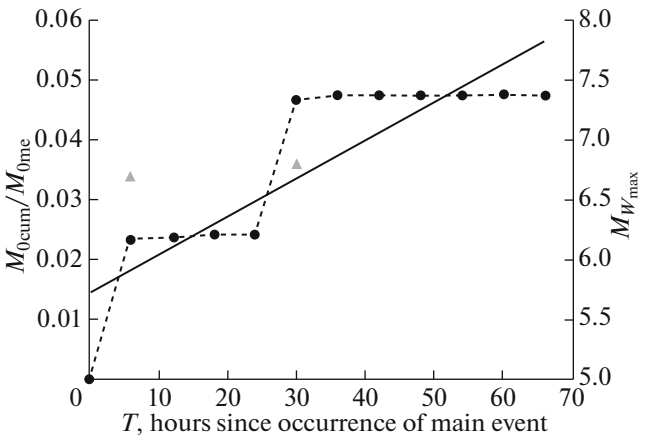

Fig. 12. Evolution of aftershock process for earthquake of April 25, 2015 in Nepal during period of April 25–27 in terms of release of scalar seismic moment (M_{0cum}). Straight line shows linear trend approximation.

is undoubtedly affected by the regional and local seismotectonic conditions under which a strong earthquake occurs.

Detection of the quasistationary phase of M_0 release makes it possible to approximate the course of release of the cumulative scalar moment during this phase with a linear dependence. Predicting the occurrence of a strong aftershock as soon as four days after the mainshock of April 25 in Nepal, we proceeded from the following ideas. The linear approximation of the initial stage of the aftershock process is shown in Fig. 12; its analytical form is

$$M_{0\text{cum aft}}/M_{0\text{ME}} = 0.0006t + 0.0144R_C = 0.867. \quad (1)$$

Here, $M_{0\text{cum aft}}$ is the cumulative scalar seismic moment released with aftershocks; $M_{0\text{ME}}$ is the scalar seismic moment of the main event; t is the time (h) counted from the moment of the mainshock; and R_C is the linear correlation coefficient.

The seismic moment of the April 25 mainshock determined in the Quick CMT [27] was $M_{0\text{ME}} = 7.76 \times 10^{20}$ N m. As of the morning of April 29, the release was $M_{0\text{cum aft}} \approx 3.69 \times 10^{19}$ N m, whereas the value estimated by formula (1) was $M_{0\text{cum aft}} \approx 5.87 \times 10^{19}$ N m. Thus, the deficit in the $M_{0\text{cum aft}}$ release was 2.17×10^{19} N m, which is equivalent to an earthquake with $M_W = 6.8$. This gave us grounds to suppose that a strong aftershock with $M_W \approx 7.0$ would occur with high probability in the aftershock zone of the Gorkha earthquake in the nearest days after April 29. On the same day, April 29, 2015, the Coordination Prediction Center of the Schmidt Institute of Physcis of the Earth, Russian Academy of Sciences, sent a corresponding message to the Center for Natural Emergency Monitoring and Prediction (Antidisaster Center), Ministry of Emergencies of the Russian Federation.

In fact, the strongest aftershock of the Gorkha earthquake occurred in the morning of May 12, 2015; according to the available data, the magnitude of its moment was 7.2 (CMT) or 7.3 (USGS, NEIC). According to formula (1), the magnitude of the moment of the aftershock, determined from the increasing deficit of M_0 release (as of the morning of May 12) was $M_W = 7.4$.

The maximum shaking intensity in the epicentral zone was VII–VIII on the modified Mercalli scale (Fig. 3b, [30]).

As seen in Fig. 13, the aftershock process in this period was completely concentrated in the eastern part of the source zone. The focal mechanism of the source was very similar to that of the mainshock of April 25 (see Fig. 8b). The types of slip in the sources of these two earthquakes were likely also similar.

Analysis of Aftershock Sequence in April–October 2015

The database for analysis of aftershock activity was the USGS catalog (NEIC), from which events with $mb \geq 3.8$ were chosen [30]. The aftershock process of the April 25, 2015 mainshock was about to end by the beginning of October 2015. The last event with $mb = 4.5$ occurred in the aftershock zone on October 5, 2015. For the period of April 25–October 5, 2015, 218 aftershocks with $mb \geq 3.9$ occurred. Figure 7 shows the map of aftershock epicenters for the mainshock of April 25 as of September 29, 2015. In addition to the events from the USGS catalog, this map also shows the epicenters of quakes recorded by GS RAS. It is seen that the latter are much less abundant: only 102 aftershocks (with $mb \geq 4.0$) of the mainshock of April 25, 2015 were listed in the catalog of SEM GS RAS for the same period. It is seen that four months after the mainshock, the aftershock zone occupies quite a large area: 26.5–31.0° N, 81.0–88.0° E. It can also be seen that the observed clusters of epicenters of relatively weak aftershocks are related both to the structures of the mainshock source and, likely, feathering seismoactive tectonic faults, for example, submeridional right-lateral strike-slips.

Almost all aftershocks, except for the strongest ones (for which M_W was determined), from the USGS catalog were characterized by magnitude mb (212 of 218). Therefore, to estimate the M_0 release with the aftershocks, the catalog was reduced to magnitude of the moment. When performing such a unification, we utilized the ratio between mb of NEIC and M_W of CMT, which was obtained for 40 events in the region that occurred in the period of 1979–2015 (mb and M_W for these events were determined simultaneously). The correlation dependence M_W (mb) is shown in Fig. 14. Its analytical form is

$$M_W = (1.177 \pm 0.114)mb - 0.852 \pm 0.682R_C = 0.863. \quad (2)$$

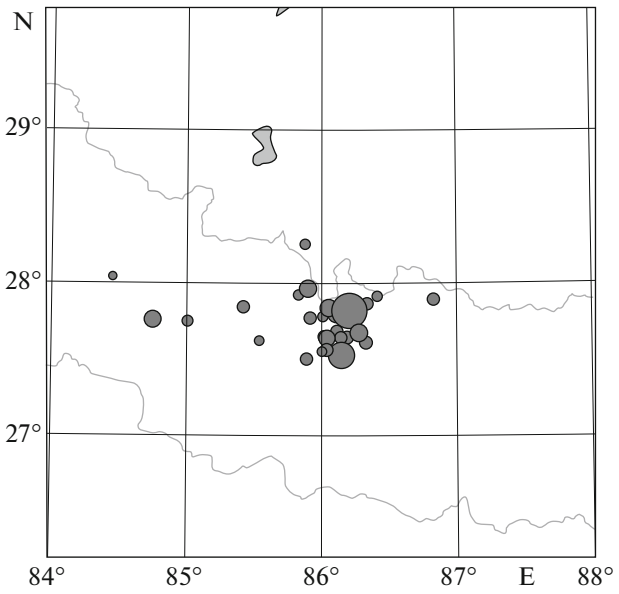

Fig. 13. Map showing epicentral locations of aftershocks for earthquake of April 25, 2015, based on data from SEM GS RAS, for period from May 2 (15:16:19 GMT) until May 13, 2015 (06:52:58 GMT). Epicenter of strongest aftershock of May 12 is shown by largest circle in eastern part of source zone. Smaller circle in same part of epicentral cloud denotes epicenter of another strong aftershock of May 12 (07:36:51 GMT, $M = 6.4$).

Transition from M_W to M_0 is done by the Kanamori formula [13].

Figure 15 shows the plot of release of the cumulative scalar seismic moment with aftershocks in fractions of the scalar seismic moment of the mainshock since its occurrence on April 25 until the beginning of October 2015. The straight line indicates regression (1), for which the magnitude of the May 12 aftershock with $M_W = 7.2$ is estimated to be $M_W = 7.4$. It can be seen from Fig. 15 that after the event of May 12, the aftershock process can be considered almost finished in terms of M_0 release. Indeed, for the period from April 25 until May 12, thr total scalar seismic moment released with aftershocks was $M_{0\text{sum}} = 1.297 \times 10^{20}$ N m, whereas for the period from May 13 until October 5, 2015, it was $M_{0\text{sum}} = 6.55 \times 10^{17}$ N m (i.e., as small as about 0.5% of the total M_0 release with aftershocks). However, 148 aftershocks ($mb \geq 3.9$) occurred for the period from April 25 until May 12, whereas 70 aftershocks occurred from May 13 until October 5, 2015 (i.e., the latter period encompassed about 1/3 of the total number of aftershocks). In this respect, such a parameter as the number of aftershocks, generally speaking, does not reflect the dynamics of the aftershock process. The total scalar seismic moment released with the aftershocks of the Gorkha earthquake of April 25, 2015 ($M_W = 7.9$) was 1.303×10^{20} N m, or 16.8% of the mainshock's scalar seismic moment.

Figure 16 depicts how M_0 was released with aftershocks along a timeline of 160 days, with a time step of $\Delta T = 10$ days.

It is seen in Fig. 15 that the duration of the quasi-stationary phase of M_0 release can be approximately estimated as 20 days. Then, the intensity of the aftershock process decreases rapidly (at about $\sim T^{-4}$) with time. This gives us grounds to think that the aftershock process of the April 25, 2015 earthquake had almost been finished, although relatively weak (but still disturbing the long-term background) seismic events could have occurred in this region for several months.

In late 2015, in an area WNW of the source zone of the Gorkha earthquake, the seismic quiescence zone formed in the High Himalayans: no moderate and weak earthquakes have been recorded here since 1993.

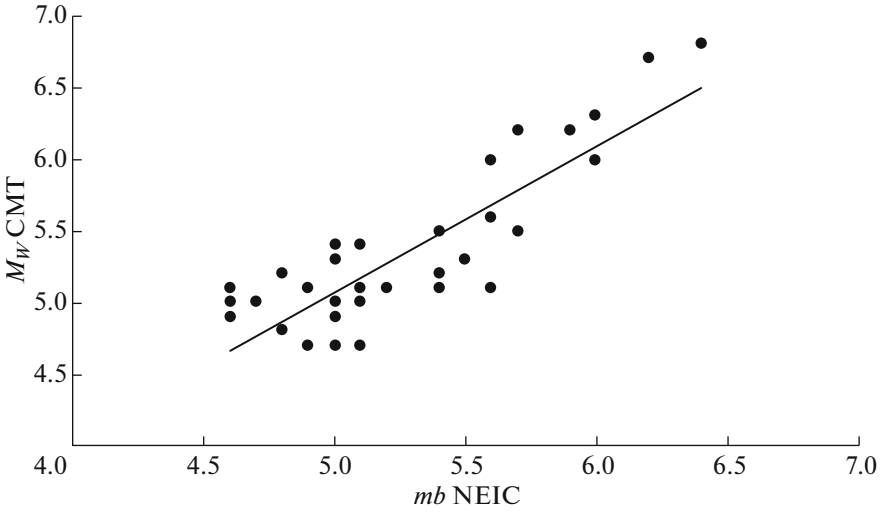

Fig. 14. Correlation dependence between M_W CMT and *mb* NEIC.

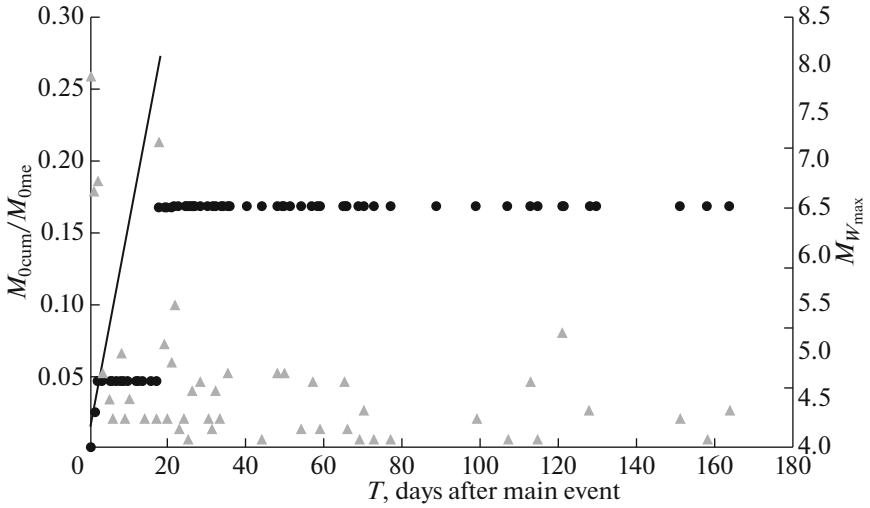

Fig. 15. Release of cumulative scalar seismic moment ($M_{0cum\ aft}$) in fractions of M_0 of main event for period from April 25 to October 5, 2015. Red triangles show magnitudes of strongest aftershock that occurred during this time interval.

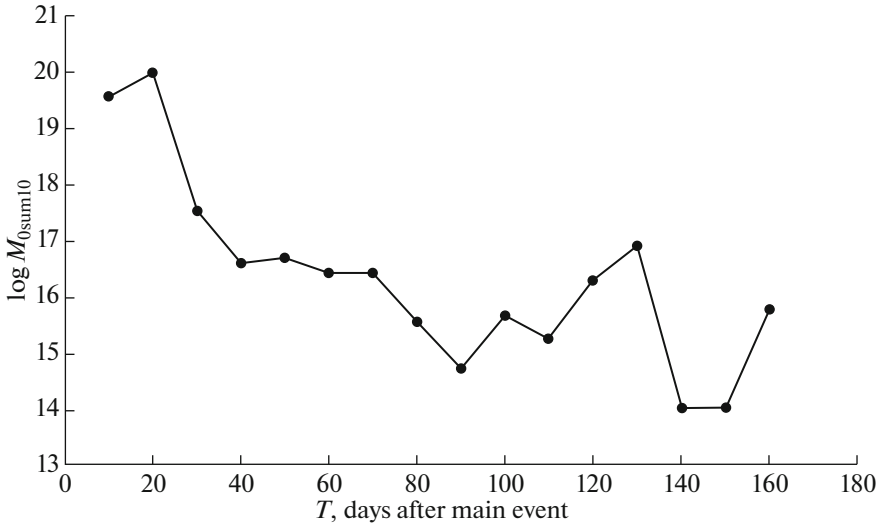

Fig. 16. Time course of M_0 release aftershocks for 160-day period after mainshock with time step of $\Delta T = 10$ days.

This seismic quiescence zone is about 250 km long and about 100 km wide and may be considered a potential source location of a future strong seismic event.

CONCLUSIONS

The strong Gorkha earthquake in Nepal had long-term seismological precursors in the form of a zone of long-term seismic quiescence.

Investigation of macroseismic effects has shown that the highest (I = VIII) isoseismal contoured the vast area in the foothills and on the southeastern slope of the High Himalayas; it had the shape of an irregular oval with the major axis oriented WNW in parallel to the direction of the mountain ranges. The length of the zone with I = VIII was about 150 km, and its width was 60–70 km.

Weaker shaking of I = VII and I = VI were reported in the entire Nepalese sector of the Himalayas and in the foothill areas of Tibet and India.

Primary seismic dislocations were not revealed on the surface. Instead, multiple secondary gravitational and vibration deformations were manifested. The earthquake triggered many rockfalls and landslides on steep slopes, vibration cracks in road pavements, local soil liquefaction, and snow avalanches in the High Himalayas. Gravitational seismic dislocations occurred

on all suitable slopes within the limits of the isoseismal with $I = \text{VIII}$.

According to the results of operational analysis of aftershock cloud formation on the first day, the earthquake source extended WNW–ESE, with linear dimensions of approximately 160–170 km in length and 50–60 km in width. Rupturing in the source began in its western part and propagated eastward. It was as though aftershocks filled the seismic quiescence zone.

The collected seismotectonic and seismological data have made it possible to construct a model of the mainshock source in the form of a plane gently dipping northward, which appeared in the zone of the Main Boundary Thrust of the Himalayas. The SSW-oriented (about 190°) horizontal displacement in different parts of the source zone during the mainshock was 1.5 to 3.5 m, while the vertical component was up to 2 m.

Operational analysis of the course of the aftershock process during the first four days after the mainshock allowed us to successfully predict the magnitude and occurrence time of the strongest aftershock of May 12, 2015.

Analysis of the aftershock sequence in April–October 2015 gives us grounds to conclude that the aftershock process of the April 25, 2015 earthquake was almost finished; however, relatively small (but still exceeding the long-term background) earthquakes in this area can occur for several months in the future.

ACKNOWLEDGMENTS

The work was supported in part by the Presidium of the Russian Academy of Sciences (Program no. 15).

REFERENCES

1. A. I. Lutikov, "Preliminary analysis of the aftershock process for the Olyutora earthquake of April 20, 2006, Koryakiya," in *The Olyutora Earthquake of April 20 (21), 2006 in the Koryak Upland: First Research Results*, Ed. by V. N. Chebrov (Geofiz. Sluzhba Ross. Akad. Nauk, Petropavlovsk-Kamchatsky, 2007), pp. 241–250.
2. A. I. Lutikov, "Evolution of the aftershock process for the earthquake of March 11, 2011 ($M_w = 9.1$) off the eastern coast of Honshu Island, Japan," in *Problems of Complex Geophysical Monitoring in the Russian Far East: Proceedings of the Third Science-and-Technical Conference, Petropavlovsk-Kamchatsky, Russia, 2011*, pp. 185–191.
3. A. A. Malovichko, I. P. Gabsatarova, M. V. Kolomiets, and L. S. Chepkunas, "The catastrophic earthquake of April 25, 2015, in Nepal: Analysis of seismological data," Seism. Instrum. **52**, 195–207 (2016).
4. L. Bollinger, S. N. Sapkota, P. Tapponnier, Y. Klinger, M. Rizza, J. Van der Woerd, D. R. Tiwari, R. Pandey, A. Bitri, and S. Bes de Berc, "Estimating the return times of great Himalayan earthquakes in eastern Nepal: Evidence from the Patu and Bardibas strands of the Main Frontal Thrust," J. Geophys. Res.: Solid Earth. **119**, 7123–7163 (2014). doi 10.1002/2014JB010970
5. U. Chandra, "Seismotectonics of Himalaya," Current Sci. **62**, 40–71 (1992).
6. D. Cheloni, "Coseismic slip model of the *M* 7.8 2015 Nepal earthquake and its *M* 7.2 aftershock from joint inversion of InSAR and GPS data," AGU Fall Meeting (2015). doi 10.13140/RG.2.1.3263.4720
7. A. Densmore, T. Dijkstra, C. Jordan, V. Banks, N. Rosser, J. Rees, G. Jenkins, and J. Williams, "Nepal: update on landslide hazard following 12 May 2015 earthquake," Earthquakes without Frontiers, British Geological Survey and Durham University, 12 May 2015. http://ewf.nerc.ac.uk/2015/05/12/nepal-update-on-landslide-hazard-following-12-may-2015-earthquake/
8. Guang-Yu Fu, Shang-Hua Gao, Guo-Qing Zhang, Ya-Wen She, and He-Ping Sun, "Gravitational isostasy background and surface deformation response characteristics of the 2015 Nepal *Ms* 8.1 earthquake," Chinese J. Geophys. **58**, 1900–1908 (2015). doi 10.6038/cjg20150606
9. J. Galetzka, D. Melgar, J. F. Genrich, J. Geng, S. Owen, E. O. Lindsey, X. Xu, Y. Bock, J. -P. Avouac, L. B. Adhikari, B. N. Upreti, B. Pratt-Sitaula, T. N. Bhattarai, B. P. Sitaula, A. Moore, et al., "Slip pulse and resonance of the Kathmandu basin during the 2015 Gorkha earthquake, Nepal," Science **349**, 1091–1095 (2015). doi 10.1126/science.aac6383
10. A. Gansser "The morphogenic phase of mountain building," in *Mountain Building Process*, Ed. by K. J. Hsu (Academic Press, London, 1982), pp. 221–228.
11. Adam Forte, Gorkha, Nepal 2015 Earthquake Visualization – 1. https://vimeo.com/126649767
12. Guohua Gu, Wuxing Wang, Yueren Xu, and Wenjun Li, "Horizontal crustal movements before the great Wenchuan earthquake obtained from GPS observations in the regional network," Earthquake Sci. **22**, 471–478 (2009).
13. H. Kanamori, "The energy release of great earthquakes," J. Geophys. Res. **82**, 2981–2987 (1977).
14. J. S. Kargel, G. J. Leonard, D. H. Shugar, U. K. Haritashya, A. Bevington, E. J. Fielding, K. Fujita, M. Geertsema, E. S. Miles, J. Steiner, E. Anderson, S. Bajracharya, G. W. Bawden, D. F. Breashears, A. Byers, et al., "Geomorphic and geologic controls of geohazards induced by Nepal's 2015 Gorkha earthquake," Science **351**, aac8353 (2016). doi 10.1126/science.aac8353
15. K. N. Khattri, "Great earthquakes, seismicity gaps and potential for earthquakes disaster along the Himalaya plate boundary," Tectonophysics **138**, 79–92 (1987).
16. J. R. Kayal "Seismicity of northeast India and surroundings—Development over the past 100 years," J. Geophys. **19**, 9–34 (1998).
17. E. O. Lindsey, R. Natsuaki, X. Xu, M. Shimada, H. Hashimoto, D. Melgar, and D. T. Sandwel, "Line of sight deformation from ALOS-2 Interferometry: *Mw* 7.8 Gorkha earthquake and *Mw* 7.3 aftershock," Geophys. Res. Lett. **42**, 6655–6661 (2015). doi 10.1002/2015GL065385
18. G. Monsalve, A. Sheehan, V. Schulte-Pelkum, S. Rajaure, M. R. Pandey, and F. Wu, "Seismicity and 1-D velocity structure of the Himalayan collision zone. Earthquakes in the crust and upper mantle," J. Geo-

phys. Res.: Solid Earth **111**, B1030110 (2006). doi 10.1029/2005JB004062

19. E. O. Lindsey, R. Natsuaki, X. Xu, M. Shimada, H. Hashimoto, D. Melgar, and D. T. Sandwel, "Nepal Earthquake: line of sight deformation from ALOS-2 interferometry," in *International Conference in Kathmandu, Nepal, 2015.*
20. P. Molnar, "A review of the seismicity and the rates of active underthrusting and deformation at the Himalaya," J. Himalayan Geol. **1**, 131–154 (1990).
21. M. R. Pandey, R. P. Tandukar, J. P. Avouac, J. Lave, and J. P. Massot, "Interseismic strain accumulation on the Himalayan crustal ramp (Nepal)," Geophys. Res. Lett. **22**, 751–754 (1995).
22. M. R. Pandey, R. P. Tandukar, J. P. Avouac, J. Vergne, and T. H. Heritier, "Seismotectonics of the Nepal Himalaya from local seismic network," J. Asian Earth Sci. **17**, 703–712 (1999).
23. E. A. Rogozhin, A. N. Ovsyuchenko, and I. A. Parvez, "Paleoseismogeological investigations in a 'Seismic Gap' in the Northwest Caucasus compared to the West Himalayan region," Seism. Instrum. **46**, 356–362 (2010).
24. J. L. Schmidt, P. K. Zeitler, F. J. Pazzaglia, M. M. Tremblay, D. L. Shuster, and M. Fox, "Knickpoint evolution on the Yarlung river: Evidence for late Cenozoic uplift of the southeastern Tibetan plateau margin," Earth Planet. Sci. Lett. **430**, 448–457 (2015).
25. K. S. Valdiya, "The two intracrustal boundary thrusts of the Himalaya," Tectonophysics **66**, 323–348 (1980).
26. K. S. Valdiya, "Tectonics and evolution of the central sector of the Himalaya," Philos. Trans. R. Soc., A **326**, 151–175 (1988).
27. Catalog of Centroid Moment Tensor, Harvard University (United States). http://www.globalcmt.org/CMTsearch.html. Accessed April 28, 2015.
28. *M* 7.8–36 km of Khudi, Nepal Earthquake Hazards Program. http://earthquake.usgs.gov/earthquakes/eventpage/us20002926. Accessed July 10, 2015.
29. Catalog of the Earthquake Early Alert Service, Geophysical Survey of the Russian Academy of Sciences. http://www.ceme.gsras.ru/ceme/. Accessed April 29, 2015.
30. Earthquake catalog of the United States Geological Survey. http://earthquake.usgs.gov/earthquakes/search. Accessed October 10, 2015.

Reviewer: V.G. Trifonov
Translated by N. Astafiev